Electrochemical Reduction of CO_2 at Au-Pd Core-Shell Nanoparticles: Product Distribution *vs.* Shell Thickness

Jo J. L. Humphrey,[a] Dr. Daniela Plana,[a] Dr. Verónica Celorrio,[a] Dr. Sajanikumari Sadasivan,[b] Dr. Robert P. Tooze,[b] Dr. Paramaconi Rodríguez,[c] and Prof. David J. Fermín[a]*

Abstract: The electrocatalytic reduction of CO_2 at carbon-supported Au-Pd core-shell nanoparticles is systematically investigated as a function of Pd shell thickness. Liquid and gas phase products were determined by off-line ^1H NMR and on-line electrochemical mass spectrometry (OLEMS). Our results uncover the relationship between the nature of products generated and the Pd shell thickness. CO and H_2 are the only products generated at 1 nm thick shells, while shells of 5 and 10 nm produced $HCOO^-$, CH_4 and C_2H_6. The concentration of $HCOO^-$ detected in the electrolyte was dependent on the applied potential, reaching a maximum Faradaic efficiency of 27% at -0.5 V *vs.* RHE for 10 nm thick shells. We conclude that collisions between absorbed hydrogen at relaxed Pd lattices and strongly bound "CO–like" intermediates promote the complete hydrogenation to C1 and C2 alkanes, without the generation of other products such as alcohols and aldehydes.

Introduction

Since the middle of the 20th century, mean annual atmospheric CO_2 levels have increased by over 25 %; in May 2014, the atmospheric concentration of CO_2 exceeded 400 ppm for the first time.[1] One of the greatest technological challenges in the energy sector is the development of effective and scalable means of transforming CO_2 into high added value products, without emitting further CO_2 into the environment. Arguably, this can only be achieved by technologies that can be powered by renewable energy sources. Electrochemical approaches offer a route to the conversion of carbon dioxide into renewable fuels, such as methanol or formic acid, under mild conditions.[2-8] Not only would this assist in alleviating the detrimental effects of accelerated global warming and climate change, but it would also facilitate the production of alternatives to fossil fuels.

[a] Miss J.J.L. Humphrey, Dr. D. Plana, Dr. V. Celorrio and Prof. D.J. Fermín*
School of Chemistry
University of Bristol
Cantocks Close, Bristol, UK, BS8 1TS
E-mail: david.fermin@bristol.ac.uk
[b] Dr. S. Sadasivan, Dr. R. P. Tooze
Sasol Technology UK Ltd.
Purdie Building, North Haugh, St. Andrews, Fife, Scotland, UK, KY16 9ST
[c] Dr. P. Rodríguez
School of Chemistry
University of Birmingham
Edgbaston, Birmingham, UK, B15 2TT

Supporting information for this article is given via a link at the end of the document.

The majority of work in this area so far has focused on the use of flat metallic cathodes to catalyse the electroreduction of CO_2.[2, 4, 5, 7, 9, 10] Hori *et al.* demonstrated that bulk Cu electrodes could be used to produce hydrocarbons, such as CH_4 and C_2H_4, with efficiencies of 65 and 20%, respectively.[2] More recently, the Jaramillo group explored the activity and selectivity towards the CO_2 reduction of a range of transition metals, employing gas chromatography and NMR techniques to detect gas and liquid phase products of CO_2 electrolysis with high sensitivity.[4, 11, 12] They suggested descriptors such as the binding energies of the CO_{ads} intermediate and O_{ads} (*i.e.* surface oxophilicity) to rationalise reactivity trends and hence tune reactivity and selectivity.[12] On the other hand, Pd has shown unique reactivity for CO_2 reduction compared to other group 10 elements, producing HCOOH at low overpotentials,[13-15] and hydrocarbons at higher overpotentials.[16] This behaviour has often been ascribed to the ability of Pd to not only adsorb hydrogen on its surface, but also absorb reactive hydrogen into its crystal lattice.[10, 13, 17, 18]

Min and Kanan reported a kinetic analysis of the electrohydrogenation of CO_2 and $KHCO_3$ at carbon-supported Pd nanoparticles, concluding that $HCOO^-$ formation proceeded with Faradaic efficiencies close to 100% in the potential range between -0.05 to -0.35 V vs. RHE.[15] In addition, the authors also reported the rapid deactivation process of the electrode associated with the formation of CO *via* a minor reaction pathway.[15] Further mechanistic studies by Kortlever *et al.* have shown the influence of pH on the CO_2 reduction reaction at Pd, Pd-Pt and Pt disc electrodes.[13] Those studies demonstrated that, at low overpotential, $HCOO^-$ could be formed at Pd electrodes either by direct reduction of CO_2 or by HCO_3^- reduction, while at higher overpotentials formic acid is produced only by direct reduction of CO_2.

Bimetallic materials offer an effective way of tailoring the electrocatalytic activity of *d*-metals, which can be rationalised in terms of the so-called ligand and strain effects.[19] Au-Pd has recently been studied as electrocatalyst for CO_2 electroreduction,[8, 20] motivated by the fact that these bi-metallic systems exhibit good activity towards HCOOH oxidation.[21, 22] Hahn *et al.* employed electron beam deposition techniques to prepare Au-Pd alloy thin films with varying atomic compositions, and demonstrated that the alloys showed improved selectivity for $HCOO^-$ compared to either Au or Pd.[20] Another level of control over the selectivity of CO_2 reduction could be achieved by growing thin Pd layers at Au surfaces. Plana *et al.* showed that the competition between CO_2 reduction and hydrogen evolution

significantly shifted towards the latter upon increasing the shell thickness in Au-Pd core-shell (CS) nanoparticles from 1 to 10 nm.[8] Januszewska *et al.* reported that CO_2 reduction becomes more hindered as the thickness of Pd overlayers on Au(111) surfaces increases due to the formation of adsorbed CO intermediates.[23]

The work presented herein examines the interplay between CO adsorption, hydride formation and the hydrogen evolution reaction on the electrochemical reduction of CO_2 at Au-Pd CS nanoparticles. Our analysis, based on off-line proton NMR and on-line electrochemical mass spectrometry (OLEMS), shows that decreasing the Pd thickness from 10 to 1 nm leads to a decrease in the Faradaic efficiency towards the generation of HCOOH, CH_4 and C_2H_6. We link this trend to a decrease in CO affinity with increasing Pd strain, as well as a decrease in the overall H population absorbed in the Pd lattice. Under the experimental conditions employed in this work, we recorded a maximum Faradaic efficiency in excess of 25% for 10 nm Pd shells at low CO_2 reduction overpotential. At more negative potentials, the Faradaic efficiency for $HCOO^-$ decreases due to an increase in the rate of H_2 evolution, as well as hydrocarbons.

Results and Discussion

Dynamic electrochemical responses as a function of Pd thickness

High-resolution TEM images shown **Figure 1a, d** and **g** show a clear contrast between Au core and Pd shell domains, as well as lattice fringes extending from the core to the shell. These data corroborate a core-shell structure, obtained by the low-temperature synthesis of these Au-Pd nanostructures. Further evidence of the nanomaterials' core-shell nature is given by the dark-field high resolution STEM-HAADF images shown in **Figures 1c**, **f** and **i**, and is particularly clear for the CS5 and CS10 particles. TEM images displayed in **Figures 1b**, **e** and **h** also show that particles are well dispersed in the Vulcan XC-72 matrix. Furthermore, these images demonstrate the monodisperse nature of the particles, and that Pd only nucleates on the Au cores.

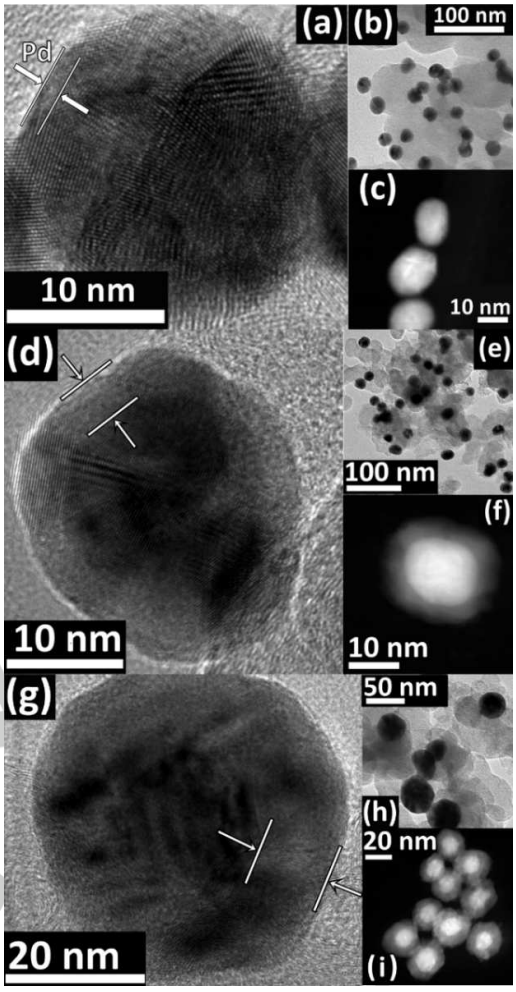

Figure 1. High-resolution TEM images of CS1 (a), CS5 (d) and CS10 (g). TEM images of CS1 (b), CS5 (f) and CS10 (h) dispersed on Vulcan XC-72R. STEM-HAADF images of CS1 (c), CS5 (f) and CS10 (i) particles. The Pd shell thickness is indicated by the arrows on the HR images.

Table 1: Structural parameters of the catalysts as analysed by HR-TEM, selected area electron diffraction and composition analysis based on EDX and AAS.

Catalyst	Shell Thickness[¥] nm	Particle Diameter[¥] nm	Metal Loading %wt	Pd Mass Ratio %wt	Effective Pd Lattice Strain[¥] %	CO_{ads} Charge Density[¥§] 0.5 M H_2SO_4 10^4 C cm^{-2}
Au	-	19.3 ± 1.2	19.5 ± 1.2	0	-	-
CS1	1.3 ± 0.9	21.8 ± 1.1	20.7 ± 3.9	16 ± 4	3.3 ± 0.6	1.6 ± 0.3
CS5	5.1 ± 0.9	29.5 ± 1.2	16.2 ± 1.6	59 ± 7	1.4 ± 0.6	3.1 ± 0.2
CS10	9.9 ± 1.1	38.9 ± 1.5	23.6 ± 4.3	82 ± 8	0.6 ± 0.6	3.6 ± 0.5

[¥] Data averaged from several hundreds of nanoparticles including those reported in ref. [21]

[§] Adsorbed CO_{ads} oxidation data are exemplified in the supporting information (Figure S1).

Table 1 summarises the main structural parameters of the metallic catalysts which are consistent with our previous studies.[21, 24, 25] Metal loadings and Au:Pd mass ratio in the catalyst layers have been quantified by atomic absorption spectroscopy (AAS) and energy dispersive x-ray spectroscopy (EDX), and are reported as an average of the two techniques. In our previous studies,[25] selected area electron diffraction patterns allowed the effective Pd strain induced by the Au cores to be estimated as a function of the average thickness; within the error margins, the Pd lattice in the 10 nm shells can be considered fully relaxed.[21, 24, 25] The mean oxidation charges of a CO monolayer at the Pd shells in 0.5 M H_2SO_4 are also included in **Table 1**. Typical voltammograms obtained for the oxidation of adsorbed CO are displayed in Figure S1, showing identical trends to those previously reported.[21] Under these conditions, the CO coverages decreases with shell thickness, a trend consistent with values obtained at Pd(111) single crystal surfaces and a pseudomorphic Pd monolayer on a Au(111) substrate.[26]

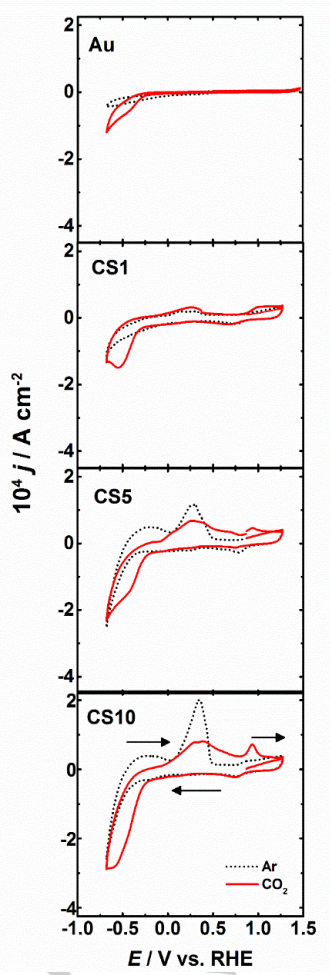

Figure 2: Cyclic voltammograms of Au and Au-Pd CS electrocatalysts recorded in Ar (black dotted) or CO_2 (red) saturated Na_2SO_4 (pH 4) at 0.020 V s^{-1}. The potential is initially swept from 0.7 V to 1.3 V, followed by scanning to -0.7 V and back to 1.3 V.

Figure 2 contrasts cyclic voltammograms of Au and Au-Pd CS nanoparticles recorded in Ar and CO_2-saturated electrolytes at pH 4. This pH ensures the maximum CO_2 concentration in aqueous solutions, minimising competing equilibria with HCO_3^- species which can also be reduced by Pd electrodes.[13] Therefore all electrochemical signals and any products formed can be directly attributed to the reduction of dissolved CO_2. In view of the pH sensitivity of the CO_2 reduction reaction, control experiments require solution pH to be the same in the absence and presence of CO_2, something which is often overlooked in the literature.[6, 23] Accordingly, the pH of Ar-saturated Na_2SO_4 was adjusted to pH 4 using 0.5 M H_2SO_4 to ensure it was the same pH as CO_2-saturated electrolyte.

In Ar-saturated electrolyte, Au nanoparticles exhibit electrochemical signals in the region 0.0 to -0.7 V, which are related to hydrogen processes, and are the only significant signals in this potential range. For the CS nanostructures, signals associated with Pd oxide formation and reduction are observed at potentials above 0.7 V. Responses associated with H-absorption, hydride formation and hydrogen evolution are observed at potentials more negative than -0.2 V. In the positive scan, signals in the range between 0.0 and 0.4 V are linked to H-desorption from the Pd surface and from within the crystal lattice. The magnitude of the hydrogen-related signals increases with increasing shell thickness, in agreement with previous studies carried out in more acidic solutions.[8, 21, 25] The Pd shells exhibit good stability upon repetitive cycles within the potential range investigated.

In CO_2-saturated electrolyte, the onset of CO_2 reduction at Au nanoparticles is located at -0.3 V. For the CS nanoparticles, significant changes can be seen as a function of the Pd thickness. In the negative-going potential scan, a clear contrast in the cathodic current can be seen upon CO_2 saturation. The onset for CO_2 reduction shifts slightly towards more positive potentials with increasing Pd thickness. A similar effect was observed for Au-Pd alloy electrodes, and linked to concomitant Pd-hydride formation, which was more facile in alloys with higher Pd content.[20] Minor cathodic peaks can be seen between 0.3 and -0.3 V for CS5 and CS10, which could be linked to the adsorption of CO_2 to the catalyst surface.[27, 28] However, the most noticeable features for the thicker Pd layers correspond to the partial suppression of the H-related responses in the positive scan up to approximately 0.4 V. In the case of Au nanoparticles and CS1, the differences in the voltammograms between Ar- and CO_2-saturated electrolytes in this potential range are rather minor. Another interesting feature observed, particularly for CS5 and CS10 catalysts, is a well-defined peak at 0.8 V in the positive scan. It should be mentioned that this peak is not observed in the initial part of the first voltammogram in the region of 0.7 to 1.25 V; systematic variation of the negative potential limit shows that the oxidation peak at 0.8 V is only observed when the potential is swept beyond the onset potential for CO_2 reduction.

The precise identity of the intermediate responsible for the voltammetric feature at 0.8 V remains to be fully elucidated, with works suggesting adsorbed CO[29] or a range of multi-bonded CO radicals, (HCOO), CHO, $C(OH)_2$ and CH_x.[6, 28, 30] For the sake of simplicity, we shall refer to this feature as "CO-like" oxidation. It is noticeable that the "CO-like" oxidation current significantly

decreases as the shell thickness decrease from 10 to 1 nm. This observation correlates well with the decrease in the CO_{ads} oxidation charge summarised in **Table 1**.[21] However, the excess anodic current in the whole potential range above 0.5 V is also noticeable, particularly for CS5 and CS10 electrocatalysts in the presence of CO_2. This excess current could be related to the oxidation of other species generated from CO_2 reduction. Indeed, Pérez-Rodríguez *et al.* suggested that CO_2 reduction at Pd nanoparticles leads to the formation of a range of adsorbed intermediates such as $HCOO_{ads}$, HCO_{ads} and CH_x species, which can be linked to the oxidation current observed in the positive going scan.[6] On the other hand, these responses can be associated with H-desorption processes which are shifted to more positive potentials due to surface-adsorbed species previously formed during CO_2 reduction.[6, 18, 31]

CO_2 electrolysis and product analysis

Figure 3a contrasts the charge density as a function time recorded during potential step measurements in the Ar and CO_2 saturated solutions for the CS1 electrocatalysts at -0.3 V. This potential corresponds to the onset of CO_2 reduction (see **Figure 2**). Interestingly, the charge density recorded in CO_2-saturated electrolyte is approximately an order of magnitude lower than in Ar-saturated solution. This result suggests that CO_2 adsorption inhibits the competing hydrogen processes.[28] **Figure 3b** illustrates the systematic increase in charge density for CO_2 electrolysis at CS1 electrocatalyst with variation in potentials from -0.3 V to -0.7 V. A significant step change in the value of the charge density is recorded at -0.7 V, suggesting a strong contribution from the hydrogen evolution reaction at these negative potentials. There was a negligible increase in the solution pH (< 0.3 pH units) for electrolysis at potentials more positive than -0.5 V. However at -0.7 V, the pH increased by up to 0.8 pH units during the course of the electrolysis for CS5 and CS10. This observation is consistent with a significant proton consumption, which is as a result of the competing hydrogen evolution reaction at the thick shell nanostructures.

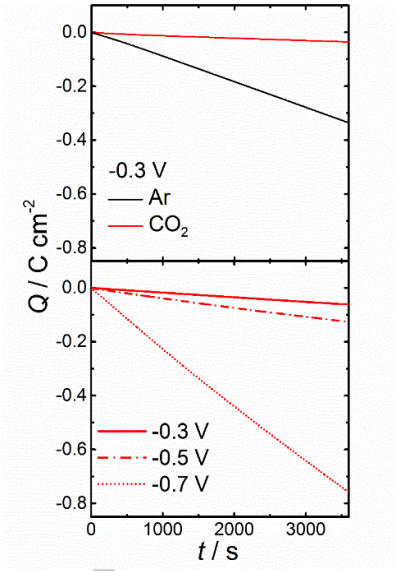

Figure 3: Charge density during electrolysis in Ar- and CO_2-saturated electrolytes at -0.3 V for CS1 catalyst (a). Charge density of CO_2 electrolysis at CS1 catalyst at various potentials (b).

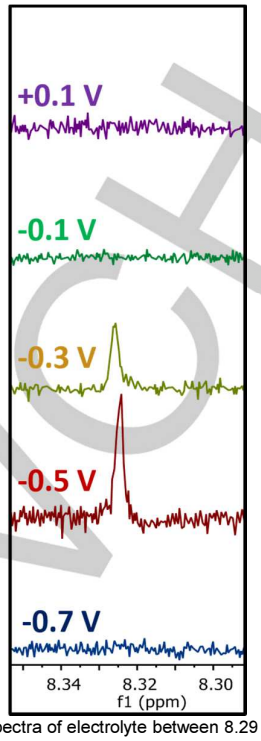

Figure 4: ^{1}H NMR spectra of electrolyte between 8.29 to 8.35 ppm following 1 h CO_2 electrolysis at potentials between +0.1 and -0.7 V at CS10 electrocatalyst. The singlet peak at 8.31 ppm is attributed to the α-proton of formate, $\underline{H}COO^-$.

Representative ^{1}H NMR spectra between 8.29 and 8.35 ppm of the electrolyte following CO_2 electrolysis with CS10 electrocatalyst are presented in **Figure 4**. At applied potentials of -0.3 and -0.5 V, there is a singlet peak at 8.31 ppm which is attributed to the α-proton of formate, $\underline{H}COO^-$. No $HCOO^-$ is detected at potentials below -0.1 V, nor at -0.7 V. These results confirm that $HCOO^-$ is formed in a narrow potential range which is consistent with previous reports.[13-15, 18, 20, 32]

Figure 5a shows the concentration of $HCOO^-$ detected in the electrolyte for the Au and CS electrocatalysts as a function of the applied potential. By keeping the sample preparation and NMR acquisition parameters consistent, it was possible to quantify the concentration of $HCOO^-$ present in the electrolyte following bulk potentiostatic CO_2 electrolysis (see Supporting Information). For Au and CS1 electrocatalysts, $HCOO^-$ was not detected by ^{1}H NMR experiments at any of the applied potentials investigated. Approximately 7 μM of $HCOO^-$ was detected at -0.3 V for CS5 nanostructures. The largest concentration of $HCOO^-$ was obtained for electrolysis with CS10 nanoparticles, yielding values close to 50 μM at -0.7 V. The corresponding Faradaic efficiencies are presented in **Figure 5b**. CS10 nanoparticles exhibit a maximum

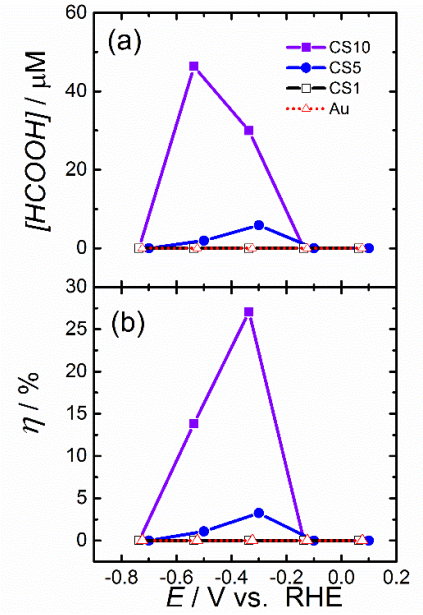

Figure 5: Concentration of $HCOO^-$ (a) and corresponding Faradaic efficiency (b) recorded after 1 hour CO_2 electrolysis at Au and Au-Pd CS nanoparticles.

Faradaic efficiency towards $HCOO^-$ of approximately 27% at potentials between -0.3 and -0.4 V, falling sharply at more negative potentials. Decreasing Pd thickness also leads to a sharp decrease in the Faradaic efficiency. The maximum Faradaic efficiencies towards $HCOO^-$ in **Figure 5b** are somewhat lower than the maximum values recently reported by Koper *et al.* (Pd-Pt alloy nanoparticles)[13, 17] and Kanan *et al.* (Pd nanoparticles)[15] in the range of 60 to 100%. On the other hand, Gao *et al.* reported very low Faradaic efficiencies (below 1% for HCOOH) for small Pd particles between 1 and 10 nm at a range of acidic pH,[33] while Hahn *et al.* obtained efficiencies of below 10% for $HCOO^-$ at alloy Au-Pd film electrodes in aqueous $KHCO_3$.[20] The range of Faradaic efficiencies reported in the literature indicate that electrode composition and nanostructuring, as well as electrolyte composition and pH, play an important role in this complex reaction.

Figure 6 shows ion currents corresponding to *m/z* 2 (H_2), 15 (CH_4) and 26 (C_2H_6) obtained by OLEMS during electrolysis with CS5 and CS10. There is a very short time delay between the current responses (**Figures 6a** and **b**) and H_2 detection (**Figures 6c** and **d**) at -0.7 V, indicating that this is the main reaction product. Interestingly, CS5 (**Figure 6e**) and CS10 (**Figure 6f**) exhibit responses associated with CH_4 and C_2H_6 species. In this case, signals relating to both CH_4 and C_2H_6 progressively increase for approximately 500 s, followed by a period of saturation and a slow decrease after 1000 s, while H_2 is also seen to decrease. This gradual decline in the activity toward hydrocarbon formation may indicate accumulation of poisoning intermediates on the electrocatalysts' surface. For CS1 and Au, CH_4 and C_2H_6 products were not detected during CO_2 electrolysis (Supporting Information Figures S3 and S4), and no CO_2 reduction products were detected when the electrolyses were performed in Ar-saturated electrolyte for any of the electrocatalysts (Supporting

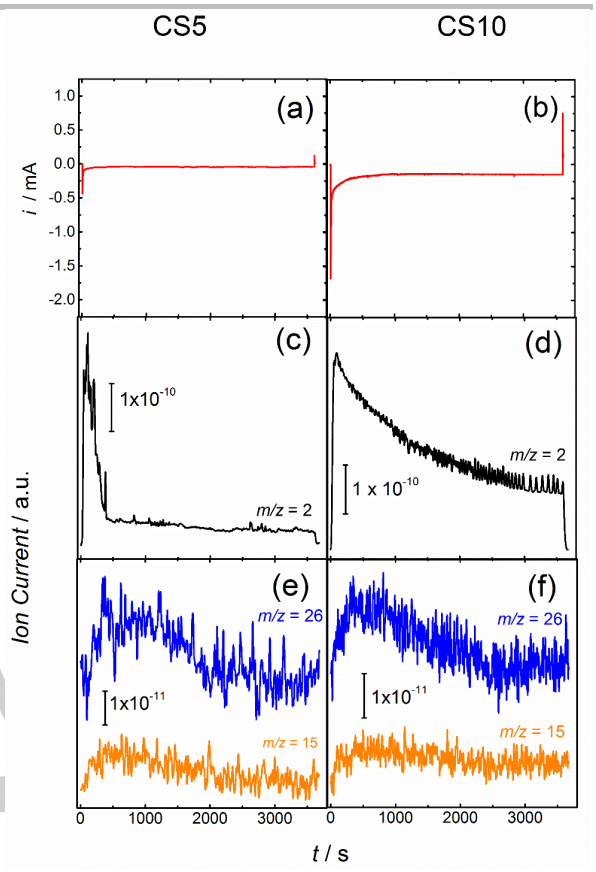

Figure 6. Faradaic and ion currents measured by OLEMS during CO_2 reduction at -0.7 V at CS5 and CS10 electrocatalysts: current (a, b), H_2 (c,d), CH_4 and C_2H_6 (e, f). All OLEMS data correspond to the ion currents measured during the course

Information Figures S5-8). It was not possible to unequivocally confirm the formation of CO with this technique, as CO can be formed as a fragment of $HCOO^-$, as well as from CO_2 itself. The *m/z* 31 fragments for methanol was also monitored, but was not detected for any catalyst. The ion currents measured for H_2 evolution are lower in CO_2-saturated electrolyte compared to Ar (Figures S6 and S7). Recently, work on Au-Cu core-shell electrocatalysts revealed a change in the distribution of gas phase CO_2 reduction products with electrolysis time, e.g. some catalysts showed a decrease of C_2H_4 generation concomitant with an increase in CH_4 formation.[34] Such changes in product distribution with electrolysis time were not seen in our systems.

Product Distribution as a Function of Shell Thickness

Scheme 1 summarises the CO_2 reduction products generated at Au and Au-Pd CS electrocatalysts. Qualitative and quantitative changes in the product distribution were observed as a function of both applied potential and catalyst composition, with Au and CS1 reducing CO_2 to CO, while CS5 and CS10 also produced $HCOO^-$ and hydrocarbons. The majority of transition metals (the exception being Cu) catalyse the $2e^-$ reduction of CO_2 to CO or $HCOO^-$, with the selectivity for each of these products dependent on the binding mode of the initial intermediate.[10, 35] It has been

proposed that CO is formed when the reaction pathway involves a Pd-C bond, *i.e.* a carboxyl intermediate, *COOH, formed by concerted proton-electron transfer.[35] Reduction of CO_2 to hydrocarbons at metal electrodes proceeds *via* further reduction along this CO pathway, by protonation of the "CO-like" species to adsorbed *COH or *CHO.[35, 36] Based on the Sabatier principle, hydrocarbons may be generated when "CO" binds strongly enough to allow further hydrogenation, yet not so strongly that the electrode is poisoned.[7] However, in most cases, reduction of CO_2 to CH_4 requires high overpotentials due to the thermodynamically unfavourable protonation step.[7, 35, 37] Formate, on the other hand, is formed *via* a separate pathway in which the initial intermediate binds to the catalyst *via* oxygen, either in a monodentate or bidentate configuration, leaving the carbon atom of CO_2 available for hydrogenation.[7, 35]

CS1 catalysts showed no formate or hydrocarbon products by NMR or OLEMS analysis, indicating a similar reactivity to pure Au nanoparticles. In the case of Au, the low oxophilicity means that CO_2 binds primarily via a Pd-carbide bond, thus inhibiting the $HCOO^-$ reduction pathway. Indeed, reports have shown Faradaic efficiencies of >85% for CO at Au electrodes in acidic electrolyte.[27, 38] Our results show that a 3.4 % expansion of the Pd lattice leads to substantial weakening of the affinity towards "CO-like" intermediates, preventing further reduction steps. This behaviour is fully consistent with the decrease in the mean CO coverage with Pd thickness shown in **Table 1**.

Both CS5 and CS10 exhibit product distributions similar to that reported for Pd electrodes, generating $HCOO^-$ at low overpotentials (between -0.3 and -0.5 V), and hydrocarbons at higher overpotentials (-0.7 V). The detection of $HCOO^-$ indicates intermediate binding of CO_2 *via* oxygen atoms, which can be protonated either by H^+ from solution, or by an insertion mechanism with ad/absorbed H.[35] Given that $HCOO^-$ was only detected for these thicker shell nanostructures, and not CS1, we speculate that the collision is between absorbed hydrogen and the surface-bound intermediate in this pathway. This step has been suggested in various studies at bulk Pd electrodes, [10, 13, 15, 17] and this conclusion is supported by the increased concentration of $HCOO^-$ produced at CS10 nanostructures, which have the highest H-absorption charge density of all the CS catalysts investigated.[25]

Both CH_4 and C_2H_6 were detected by OLEMS. While Au-Pd CS electrocatalysts have higher tolerance to CO poisoning than pure Pd,[21, 39] this intermediate still binds strongly. At CS5 and CS10, the more relaxed Pd shells facilitate binding of the "CO-like" intermediate, increasing the probability of undergoing further hydrogenation with readily available absorbed H. Based on models describing carbon-carbon coupling at Cu electrodes, the pathway for the formation of C2 hydrocarbon at Pd electrodes can be described in terms of two processes: (1) dimerization of intermediates produced on the C1 (methane) pathway,[40] or by a bi-molecular surface reaction involving "CO-like" species.[41] The high overpotentials required to generate hydrocarbons at Pd electrodes may indicate that the dimerization pathway is the most likely mechanism for the formation of C2 species. This is also consistent with fact that no other products such as acetate or acetaldehyde are detected in our studies.

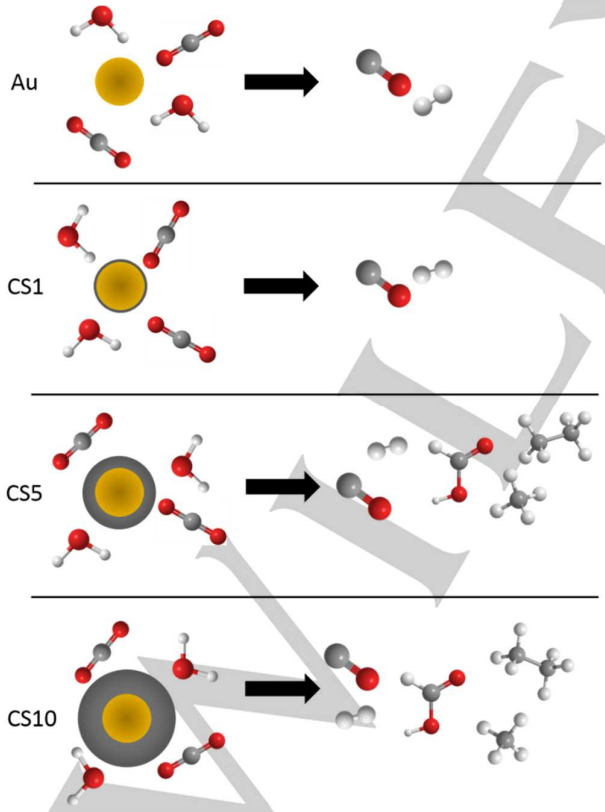

Scheme 1. Qualitative summary of CO_2 reduction products generated at Au and Au-Pd CS nanostructures.

Conclusions

The present study shows that the efficiency and product selectivity of CO_2 electroreduction at thin Pd shells is determined by two key parameters: (i) H absorption (Pd hydride formation) and (ii) CO adsorption, with both parameters strongly linked to shell thickness. Increasing Pd shell thickness from 1 to 10 nm leads to a change of product formation from CO and H_2 to a more complex distribution including CH_4, C_2H_6 and $HCOO^-$. A maximum Faradaic efficiency of more than 25% towards $HCOO^-$ is obtained at nanoparticles with 10 nm thick Pd shells. This suggests that $HCOO^-$ is the most dominant product of the CO_2 reaction, considering that previous studies under identical conditions have concluded that the overall Faradaic efficiency for CO_2 reduction at these particles is about 40% (with the remaining 60% linked to hydrogen evolution).[8] Increasing the Pd shell thickness on Au cores on this length scale leads not only to an increase in the amount of hydride formed per particle, but also to a decrease in the Pd effective lattice strain and an increase in CO affinity (see **Table 1:** Structural parameters of the catalysts as analysed by HR-TEM, selected area electron diffraction and composition analysis based on EDX and AAS.). Consequently, CO and H_2 are preferentially generated at the 1 nm shell nanoparticles due to the weaker CO affinity. As the Pd shell thickness is increased to 5 and 10 nm, lattice relaxation and increased CO affinity, along with increased H-absorption charge density, enable hydrocarbon formation. Given that no partially hydrogenated species, such as alcohols or aldehydes, are detected, we suggest that multiple electron-proton transfer steps are effectively mediated by Pd

hydride promoting fast surface hydrogenation reactions. The lack of partially reduced species also indicates that the production of $HCOO^-$ at CS5 and CS10 occurs *via* an alternative reaction pathway, in which CO_2 binds *via* oxygen, as opposed to carbon. The peak concentration of $HCOO^-$ detected at CS10 nanostructures was more than 6-times that obtained for CS5, indicating that a fine balance between "CO-like" adsorption and Pd-hydride formation is required with respect to controlling not only the product distribution, but also the efficiency, of electrochemical CO_2 reduction.

Experimental Section

Electrocatalyst Synthesis and Characterisation

Synthesis of Au-Pd CS nanoparticles by a two-step colloidal method, and their subsequent anchoring at a mesoporous carbon support (Vulcan XC-72R), has been described in previous publications.[25] [21, 25] Briefly, 19 nm diameter Au seeds were prepared by refluxing gold (III) chloride trihydrate in the presence of trisodium citrate. Pd overlayers were subsequently grown onto the Au cores by addition of aqueous H_2PdCl_4 in an ice bath with vigorous stirring, followed by L-ascorbic acid over 1 h to ensure the formation of CS, as opposed to separate Pd clusters. The thickness of the Pd shells was controlled by the volume of the Pd-precursor solution added to the colloidal Au nanoparticles. Finally the electrocatalyst was prepared by stirring the aqueous suspension of nanoparticles at room temperature in the presence of Vulcan for 3 days.

Elemental composition and metal loading of the electrocatalysts was determined by atomic absorption spectroscopy and energy dispersive X-ray spectroscopy (EDX). For AAS, carbon-supported CS nanoparticles were digested in aqua regia and diluted to 25 mL. The sample was analysed on a Unicam 919 AAS, calibrated with Au and Pd standards. EDX was performed on a JEOL SEM IT300 operating at 30 kV.

Samples for transmission electron microscopy (TEM) were prepared by drop-casting 10 µL electrocatalyst suspension in EtOH onto a 3 mm carbon-coated Cu grid (300 mesh) and drying in air. TEM imaging was carried out on a JEOL JEM 1200 EX MkII, and high-resolution TEM (HR-TEM) was carried out on a JEOL 200 Kv Hi Resolution TEM 2011, with the imaging software 'Soft Imaging Systems GmbH analySIS 3.0'. High-angle annular dark-field scanning transmission electron microscopy (STEM-HAADF) images and EDX analysis were performed in a FEI Tecnai F30, equipped with a field emission gun working at 300 kV.

Electrode Preparation and Electrochemical Studies

Catalyst inks were prepared by mixing 2.0 mg of the nanoparticle-loaded carbon with 15 µL of Nafion© perfluorinated proton exchange membrane (5 %wt, Sigma Aldrich) in 500 µL MilliQ water (≥18.2 MΩ), and sonicating to obtain a homogeneous dispersion.[21] The working electrodes were prepared by drop-casting 20 µL of ink onto a freshly polished glassy carbon electrode (5 mm diameter) and dried in air. Electrocatalysts were first activated to remove any residual surface-bound stabilising ligands by cycling the potential between -0.85 and +1.50 V (vs. RHE) at 0.500 V s^{-1} in Ar-saturated electrolyte, until stable voltammograms were obtained.

Electrochemical experiments were performed on a µAutolab potentiostat, controlled by GPES software. Currents were normalised by the electrochemically active surface area based on our previous studies employing Au oxide formation, CO adsorption and hydrogen adsorption/absorption in acid solution (see Figure S1).[21, 25] Measurements were carried out in 0.1 M Na_2SO_4 as the background electrolyte, adjusted to pH 4 by the addition of high purity H_2SO_4. The pH was measured before and after the electrolysis. Although a number of buffers were investigated, all produced electrochemical signals in the potential range of CO_2 reduction. Furthermore, some buffers can severely compromise the sensitivity of ^1H NMR measurement in a critical range of chemical shifts.

A two compartment electrochemical cell was used separating the working and Hg/Hg_2SO_4 (MSE) reference electrodes from the counter electrode (Pt) by a glass frit. All potentials were subsequently transformed to RHE. The uncompensated resistance (R_u) in this configuration is typically bellow 100 Ω, thus iR_u potential drop are insignificant under the conditions investigated. For electrolysis experiments, the total cell volume was 15.0 mL, with 7.5 mL in each compartment. Fresh electrolyte was used for each measurement.

Detection and Quantification of CO_2 Electroreduction Products

Liquid phase electrolysis products were quantified by 1D ^1H nuclear magnetic resonance (NMR) spectroscopy employing an Agilent VNMRS 500MHz spectrometer using a pre-saturation pulse sequence centred on the water peak. A 700 µL aliquot of the electrolyte was sampled from the working half of the cell with an added 35 µL of D_2O (99.9 atom % D). The concentration of $HCOO^-$ in the electrolyte following CO_2 electrolysis was determined by comparing the absolute integral of the peak area associated with $HCOO^-$ (8.31 ppm), with that of known standards. Further details regarding NMR experimental protocol and calibration (Figure S2) are provided in the Supporting Information. NMR spectroscopy results also showed trace amounts of methanol. However, this species was also detected when electrolysis was performed in the absence of CO_2, and is thought to be due to minor degradation of the carbon support under electrolysis conditions. This was confirmed by the fact that no MeOH was detected by on-line OLEMS, where Vulcan was not present.

Detection of gas phase products was performed with a custom built OLEMS system, featuring a small Kel-F tip supporting a Teflon cylinder. The tip is placed close to the electrode surface, allowing the detection of volatile products with a quadrupole mass analyser. The tip is a 1.2 mm diameter porous Teflon cylinder (Porex with an average pore size of 5 µm - 10 µm and 45 - 55 % porosity) in a Kel-F holder. The tip configurations were cleaned overnight in a solution of 2 M NaOH solution (VWR, EMSURE) and rinsed 5 times with ultrapure warm water before use. A secondary electron multiplier (SEM) voltage of 2100 V was used, except for hydrogen (*m/z* = 2) where a voltage of 1134 V was used. The pressure was equilibrated for 1 h prior to each measurement. The results presented in this work have been baseline corrected and the water partial pressure contribution subtracted.

In order to avoid any contribution of the oxidation/reduction of the citrate stabilising agents, the unsupported colloidal Au or Au-Pd CS nanoparticles solutions were washed first 3 times with a mixture 50:50 ultrapure water/ethanol (Fisher Scientific, analytical grade and centrifuged at 3000 rpm for 10 min), and then another 4 times with ultrapure water. The resulting solution of nanoparticles was re-dispersed in 5 mL ultrapure water, drop-cast onto a glassy carbon electrode and dried in an oven at 40°C. Electrolysis experiments were performed by applying a potential of -0.73 V for 1 h in both Ar- and CO_2-saturated electrolyte. The following mass fragments (*m/z*) were monitored during the electrolyses: 2 (H_2), 15 (CH_4), 26 (C_2H_6), 29 (CO), 31 (CH_3OH), 46 (HCOOH) and 44 (CO_2).

Acknowledgements

The authors are grateful to Sasol Technology (UK) Ltd. and NERC for funding, and Cabot Corp. for provision of Vulcan XC-72R. V.C.

gratefully acknowledges the Royal Society and the UK National Academy by the support though the Newton International Fellows program. D.P. and D.J.F. gratefully acknowledge the EPSRC (EP/K007025/1) for funding. P.R. acknowledges the University of Birmingham for the financial support through the Birmingham fellowship program. We also acknowledge the contributions of Dr. M. G. Montes de Oca to catalyst synthesis, and the support of Mr. J. A. Jones, Mr. L. D. Hall and Mr. D.A. Davis for assistance with materials characterisation. We acknowledge R. Fernandez-Pacheco (Instituto Universitario de Nanociencias de Aragón, INA) and M.J. Lazaro (Instituto de Carboquimica, CSIC) for their support with the characterization of nanostructures by electron microscopy. EDX and TEM studies were carried out at the Chemical Imaging Facility, University of Bristol, with equipment funded by UoB and EPSRC (EP/K035746/1 and EP/M028216/1). Finally, we thank Dr. C.P. Butts and Mr. P.G. Lawrence for their essential input with NMR spectroscopy.

Keywords: Carbon Dioxide, Electrocatalysis, Hydrogenation, Palladium, Structure-Activity Relationships

[1] P. Tans, R. Keeling, *Vol. 2015*, http://www.esrl.noaa.gov/gmd/ccgg/trends/, **2015**.

[2] Y. Hori, K. Kikuchi, S. Suzuki, *Chemistry Letters* **1985**, *14*, 1695-1698.

[3] A. Del Castillo, M. Alvarez‐Guerra, A. Irabien, *AIChE Journal* **2014**, *60*, 3557-3564; M. Le, M. Ren, Z. Zhang, P. T. Sprunger, R. L. Kurtz, J. C. Flake, *Journal of The Electrochemical Society* **2011**, *158*, E45-E49; D. T. Whipple, P. J. A. Kenis, *The Journal of Physical Chemistry Letters* **2010**, *1*, 3451-3458; C. D. Windle, R. N. Perutz, *Coordination Chemistry Reviews* **2012**, *256*, 2562-2570; A. Chen, C. Ostrom, *Chemical Reviews* **2015**, *115*, 11999-12044.

[4] T. Hatsukade, K. P. Kuhl, E. R. Cave, D. N. Abram, T. F. Jaramillo, *Physical Chemistry Chemical Physics* **2014**, *16*, 13814-13819.

[5] Y. Hori, C. G. Vayenas, R. E. White, M. E. Gamboa-Aldeco, *Vol. 42*, Springer New York, **2008**, pp. 89-189.

[6] S. Pérez-Rodríguez, N. Rillo, M. J. Lázaro, E. Pastor, *Applied Catalysis B: Environmental* **2015**, *163*, 83-95.

[7] A. A. Peterson, J. K. Norskov, *Journal of Physical Chemistry Letters* **2012**, *3*, 251-258.

[8] D. Plana, J. Florez-Montano, V. Celorrio, E. Pastor, D. J. Fermin, *Chemical Communications* **2013**, *49*, 10962-10964.

[9] W. J. Durand, A. A. Peterson, F. Studt, F. Abild-Pedersen, J. K. Norskov, *Surface Science* **2011**, *605*, 1354-1359; M. Gattrell, N. Gupta, A. Co, *Journal of Electroanalytical Chemistry* **2006**, *594*, 1-19.

[10] M. Jitaru, D. A. Lowy, M. Toma, B. C. Toma, L. Oniciu, *Journal of Applied Electrochemistry* **1997**, *27*, 875-889.

[11] K. P. Kuhl, E. R. Cave, D. N. Abram, T. F. Jaramillo, *Energy & Environmental Science* **2012**, *5*, 7050-7059.

[12] K. P. Kuhl, T. Hatsukade, E. R. Cave, D. N. Abram, J. Kibsgaard, T. F. Jaramillo, *Journal of the American Chemical Society* **2014**, *136*, 14107-14113.

[13] R. Kortlever, C. Balemans, Y. Kwon, M. T. M. Koper, *Catalysis Today* **2015**, *244*, 58-62.

[14] G. Lu, H. Wang, Z. Y. Bian, X. Liu, *Journal of Nanoscience and Nanotechnology* **2014**, *14*, 7097-7103.

[15] X. Min, M. W. Kanan, *Journal of the American Chemical Society* **2015**, *137*, 4701-4708.

[16] M. Azuma, K. Hashimoto, M. Watanabe, T. Sakata, *Journal of Electroanalytical Chemistry and Interfacial Electrochemistry* **1990**, *294*, 299-303; H. Noda, S. Ikeda, Y. Oda, K. Imai, M. Maeda, K. Ito, *Bulletin of the Chemical Society of Japan* **1990**, *63*, 2459-2462.

[17] R. Kortlever, I. Peters, S. Koper, M. T. M. Koper, *ACS Catalysis* **2015**, *5*, 3916-3923.

[18] K. Ohkawa, K. Hashimoto, A. Fujishima, Y. Noguchi, S. Nakayama, *Journal of Electroanalytical Chemistry* **1993**, *345*, 445-456.

[19] D. M. Alonso, S. G. Wettstein, J. A. Dumesic, *Chemical Society Reviews* **2012**; V. Baglio, A. Stassi, A. Di Blasi, C. D'Urso, V. Antonucci, A. S. Aricò, *Electrochimica Acta* **2007**, *53*, 1360-1364; S. Koh, P. Strasser, *Journal of the American Chemical Society* **2007**, *129*, 12624-12625; V. R. Stamenkovic, B. S. Mun, M. Arenz, K. J. Mayrhofer, C. A. Lucas, G. Wang, P. N. Ross, N. M. Markovic, *Nature materials* **2007**, *6*, 241-247; Z. Wei, J. Sun, Y. Li, A. K. Datye, Y. Wang, *Chemical Society Reviews* **2012**.

[20] C. Hahn, D. N. Abram, H. A. Hansen, T. Hatsukade, A. Jackson, N. C. Johnson, T. R. Hellstern, K. P. Kuhl, E. R. Cave, J. T. Feaster, T. F. Jaramillo, *Journal of Materials Chemistry A* **2015**, *3*, 20185-20194.

[21] M. G. Montes de Oca, D. Plana, V. Celorrio, M. J. Lazaro, D. J. Fermín, *The Journal of Physical Chemistry C* **2011**, *116*, 692-699.

[22] M. D. Obradović, S. L. Gojković, *Electrochimica Acta* **2013**, *88*, 384-389; G. Zhang, Y. Wang, X. Wang, Y. Chen, Y. Zhou, Y. Tang, L. Lu, J. Bao, T. Lu, *Applied Catalysis B: Environmental* **2011**, *102*, 614-619; W. Zhou, J. Y. Lee, *Electrochemistry Communications* **2007**, *9*, 1725-1729.

[23] A. Januszewska, R. Jurczakowski, P. J. Kulesza, *Langmuir* **2014**, *30*, 14314-14321.

[24] H. Kumarakuru, D. Cherns, M. M. de Oca, D. Fermin, in *Journal of Physics: Conference Series, Vol. 371*, IOP Publishing, **2012**, p. 012025.

[25] M. G. Montes de Oca, H. Kumarakuru, D. Cherns, D. J. Fermín, *The Journal of Physical Chemistry C* **2011**, *115*, 10489-10496.

[26] A. M. El-Aziz, L. A. Kibler, *Journal of Electroanalytical Chemistry* **2002**, *534*, 107-114; M. Hara, U. Linke, T. Wandlowski, *Electrochimica Acta* **2007**, *52*, 5733-5748.

[27] Y. Hori, H. Wakebe, T. Tsukamoto, O. Koga, *Electrochimica Acta* **1994**, *39*, 1833-1839.

[28] M. Łukaszewski, H. Siwek, A. Czerwiński, *Journal of Solid State Chemistry* **2009**, *13*, 813-827.

[29] M. W. Breiter, *Electrochimica Acta* **1967**, *12*, 1213-1218; M. W. Breiter, *Journal of Electroanalytical Chemistry and Interfacial Electrochemistry* **1968**, *19*, 131-136.

[30] D. Kolbe, W. Vielstich, *Electrochimica Acta* **1996**, *41*, 2457-2460; D. C. Papageorgopoulos, F. A. de Bruijn, *Journal of the Electrochemical Society* **2002**, *149*, A140-A145; B. Beden, A. Bewick, M. Razaq, J. Weber, *Journal of Electroanalytical Chemistry and Interfacial Electrochemistry* **1982**, *139*, 203-206; V. Kamath, H. Lal, *Journal of Electroanalytical Chemistry and Interfacial Electrochemistry* **1968**, *19*, 137-145; V. E. Kazarinov, V. N. Andreev, A. V. Shlepakov, *Electrochimica Acta* **1989**, *34*, 905-913.

[31] M. Grden, A. Paruszewska, A. Czerwinski, *Journal of Electroanalytical Chemistry* **2001**, *502*, 91-99; A. Czerwinski, S. Zamponi, R. Marassi, *Journal of Electroanalytical Chemistry* **1991**, *304*, 233-239.

[32] B. Podlovchenko, E. Kolyadko, S. Lu, *Journal of Electroanalytical Chemistry* **1994**, *373*, 185-187.

[33] D. Gao, J. Wang, H. Wu, X. Jiang, S. Miao, G. Wang, X. Bao, *Electrochemistry Communications* **2015**, *55*, 1-5; D. Gao, H. Zhou, J. Wang, S. Miao, F. Yang, G. Wang, J. Wang, X. Bao, *Journal of the American Chemical Society* **2015**, *137*, 4288-4291.

[34] J. Monzo, Y. Malewski, R. Kortlever, F. J. Vidal-Iglesias, J. Solla-Gullon, M. T. M. Koper, P. Rodriguez, *Journal of Materials Chemistry A* **2015**, *3*, 23690-23698.

[35] R. Kortlever, J. Shen, K. J. P. Schouten, F. Calle-Vallejo, M. T. Koper, *The Journal of Physical Chemistry Letters* **2015**.

[36] C. Shi, H. A. Hansen, A. C. Lausche, J. K. Norskov, *Physical Chemistry Chemical Physics* **2014**, *16*, 4720-4727.

[37] C. Shi, H. A. Hansen, A. C. Lausche, J. K. Nørskov, *Physical Chemistry Chemical Physics* **2014**, *16*, 4720-4727.

[38] Y. Hori, A. Murata, K. Kikuchi, S. Suzuki, *Journal of the Chemical Society, Chemical Communications* **1987**, 728-729; Y. Chen, C. W. Li, M. W. Kanan, *Journal of the American Chemical Society* **2012**, *134*, 19969-19972; G. B. Stevens, T. Reda, B. Raguse, *Journal of Electroanalytical Chemistry* **2002**, *526*, 125-133; W. Zhu, R. Michalsky, O. n. Metin, H. Lv, S. Guo, C. J. Wright, X. Sun, A. A. Peterson, S. Sun, *Journal of the American Chemical Society* **2013**, *135*, 16833-16836.

[39] V. Celorrio, M. G. Montes de Oca, D. Plana, R. Moliner, M. J. Lázaro, D. J. Fermín, *The Journal of Physical Chemistry C* **2012**, *116*, 6275-6282.

[40] X. Nie, M. R. Esopi, M. J. Janik, A. Asthagiri, *Angewandte Chemie International Edition* **2013**, *52*, 2459-2462; J. H. Montoya, A. A. Peterson, J. K. Nørskov, *ChemCatChem* **2013**, *5*, 737-742.

[41] F. Calle‐Vallejo, M. Koper, *Angewandte Chemie* **2013**, *125*, 7423-7426; J. H. Montoya, C. Shi, K. Chan, J. K. Norskov, *The Journal of Physical Chemistry Letters* **2015**.

[42] S. Trasatti, O. A. Petrii, *Journal of Electroanalytical Chemistry* **1992**, *327*, 353-376.

FULL PAPER

Efficiency and selectivity of CO_2 reduction is tuned by controlling the shell thickness of Au-Pd core-shell nanoparticle electrocatalysts. Varying the Pd thickness affects binding of key intermediates, including “CO-like” species and absorbed H, which in turn influence product distribution.

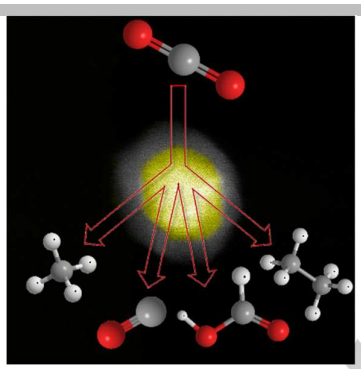

*Jo J. L. Humphrey,[a] Dr. Daniela Plana,[a] Dr. Verónica Celorrio,[a] Dr. Sajanikumari Sadasivan,[b] Dr. Robert P. Tooze,[b] Dr. Paramaconi Rodríguez,[c] and Prof. David J. Fermín[a]***

Page No. – Page No.

Electrochemical Reduction of CO_2 at Au-Pd Core-Shell Nanoparticles: Product Distribution *vs.* Shell Thickness